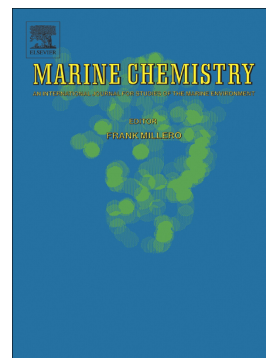


## Accepted Manuscript

Oceanic fronts control the distribution of dissolved barium in the Southern Ocean

Kimberley M. Pyle, Katharine R. Hendry, Robert M. Sherrell, Oliver Legge, Andrew J. Hind, Dorothee Bakker, Hugh Venables, Michael P. Meredith



PII: S0304-4203(18)30077-X  
DOI: doi:[10.1016/j.marchem.2018.07.002](https://doi.org/10.1016/j.marchem.2018.07.002)  
Reference: MARCHE 3569  
To appear in: *Marine Chemistry*  
Received date: 29 March 2018  
Revised date: 29 June 2018  
Accepted date: 2 July 2018

Please cite this article as: Kimberley M. Pyle, Katharine R. Hendry, Robert M. Sherrell, Oliver Legge, Andrew J. Hind, Dorothee Bakker, Hugh Venables, Michael P. Meredith , Oceanic fronts control the distribution of dissolved barium in the Southern Ocean. *Marine Chemistry* (2018), doi:[10.1016/j.marchem.2018.07.002](https://doi.org/10.1016/j.marchem.2018.07.002)

This is a PDF file of an unedited manuscript that has been accepted for publication. As a service to our customers we are providing this early version of the manuscript. The manuscript will undergo copyediting, typesetting, and review of the resulting proof before it is published in its final form. Please note that during the production process errors may be discovered which could affect the content, and all legal disclaimers that apply to the journal pertain.

*Oceanic fronts control the distribution of dissolved barium in the Southern Ocean*

Kimberley M. Pyle<sup>1</sup>, Katharine R. Hendry<sup>1\*</sup>, Robert M. Sherrell<sup>2</sup>, Oliver Legge<sup>3</sup>, Andrew J. Hind<sup>3</sup>, Dorothee Bakker<sup>3</sup>, Hugh Venables<sup>4</sup> and Michael P. Meredith<sup>4</sup>

<sup>1</sup> School of Earth Sciences, University of Bristol, Wills Memorial Building, Queen's Road, Bristol, BS8 1RJ, UK

<sup>2</sup> Department of Marine and Coastal Sciences and Department of Earth and Planetary Sciences, Rutgers University, New Jersey, USA

<sup>3</sup> Centre for Ocean and Atmospheric Sciences, School of Environmental Sciences, University of East Anglia, Norwich, NR4 7TJ, UK

<sup>4</sup> British Antarctic Survey, High Cross, Madingley Road, Cambridge, CB3 0ET, UK

\*Corresponding author

## Abstract

The globally-observed relationship between oceanic barium and the macronutrient silicic acid results from the shared influence of large-scale ocean circulation and mixing on the two elements, and the inherent link between barium and organic matter formation and dissolution. A detailed examination of deviations from barium-silicon correlations can reveal variations in non-conservative processes within the marine barium cycle. Here, we present a high-resolution dataset of dissolved barium and macronutrients from the Drake Passage and the Scotia and Weddell Seas. Our new results highlight the influence of Southern Ocean frontal zones on barium cycling and the deviations of barium and macronutrient distributions as a result of spatial variations in phytoplankton assemblages and in barite formation processes. These new data also reinforce findings that water mass mixing and ocean circulation, in particular the location of oxygen minima, play a key role in barium distribution. Our findings have implications for the use of sedimentary barium as a proxy for export production, which may be complicated by physical water circulation changes or shifts in plankton community structure.

## 1. Introduction

The oceanic barium cycle has inherent links with biological activity and carbon cycling. There is a strong positive correlation between dissolved barium ( $Ba_d$ ) and silicic acid throughout the global ocean, and a similar trend between  $Ba_d$  and alkalinity (e.g. Hoppema et al., 2010; Jacquet et al., 2005; Jacquet et al., 2007; Jacquet et al., 2008; Jeandel et al., 1996; Jullion et al., 2017; Thomas et al., 2011), likely a result of relatively deep release of Ba during particulate organic matter remineralization, coupled with large scale ocean circulation (Bates et al., 2017; Horner et al., 2015; Jeandel et al., 1996; Lea, 1993). Water column, sediment trap, and core top studies have also revealed a relationship between excess barium in the particulate phase (total barium corrected for lithogenic input,  $Ba_{xs}$ ) and particulate organic carbon (POC) (Cardinal et al., 2005). Despite the lack of a known biological requirement for Ba, high concentrations of Ba are found in phytoplankton of many taxa (Fisher et al., 1991), and barite precipitation in the water column is thought to be biologically mediated (Bishop, 1988; Collier and Edmond, 1984; Dehairs et al., 1980; Dymond et al., 1992). In microenvironments formed by phytoplankton cell walls and shell material, Ba binds with transparent exopolymer particles (TEP), cell wall associated polysaccharides or bacterial biofilm extracellular polymeric substances (EPS) (Martinez-Ruiz et al., 2018), before reacting with sulphate derived largely from seawater, to form barite (e.g. Ganeshram et al., 2003 and references therein). This organic aggregate model of barite precipitation in supersaturated microenvironments associated with decaying organic matter accounts for the distributions of barite microcrystals in mesopelagic waters (Dehairs et al., 2008; Sternberg et al., 2005), and its correlation with organic carbon in underlying sediments (Cardinal et al., 2005; Dymond et al., 1992). However, there are still unanswered questions concerning the initial associations of barium with POC in surface waters, the importance of basin-scale correlations between  $Ba_d$  and silicic acid in comparison to relationships to other macronutrients, and the mechanisms of initial Ba uptake into euphotic zone organic matter.

The Southern Ocean is of particular interest in developing our understanding of the oceanic barium biogeochemical cycle, as a climatically-important region with a large role in ocean carbon storage (Marinov et al., 2008). The potential applications of marine barite and biogenic calcite Ba/Ca as palaeo-proxies for export production and deep water circulation respectively in this region (Jacquet et al., 2007; Jacquet et al., 2008; Lea and Boyle, 1989; Nurnberg et al., 1997) make it crucial that the controls on the barium cycle in these waters are better understood. The heterogeneity of the Southern Ocean, exemplified by the biogeographical zonation caused by the convoluted and meandering circumpolar frontal zones, also offers an opportunity to investigate the various potential effects of different ecological

communities on barium distributions, and the interactions of large and small scale water-mass mixing. In the Scotia Sea, the compression of the frontal zones by the physical restrictions of the Drake Passage, and the influence of the North and South Scotia Ridges on the movement of water masses and biological activity, makes this an ideal region in which to examine the barium biogeochemical cycle. Here, we investigate the variability in the  $Ba_d$  distribution and its relationship to biological activity across the biogeochemical divide of the Polar Frontal Zone, and use these data to inform interpretations of the widely observed correlation observed between  $Ba_d$  and silicic acid. Our results reveal that site-specific deviations from a regional  $Ba_d/Si(OH)_4$  regression can be used to trace distinct water masses, and potentially to assess the degree of barite precipitation and dissolution occurring in different regions.

## 2. Methods and materials

### 2.1. Oceanographic Setting

The circulation of the Scotia Sea is dominated by the Antarctic Circumpolar Current (ACC), a wind-driven current that flows eastwards around the Antarctic continent, transporting approximately 130–140 Sv (Cunningham et al., 2003). The transport enabled by the ACC is dominated by several frontal jets identified by large horizontal gradients in oceanic properties, namely (north to south) the Subantarctic Front, the Polar Front, the Southern ACC Front and the Southern Boundary (Orsi et al., 1995) (Fig. 1). Whilst these fronts are consistently observed in the narrow constriction of the Drake Passage, at other longitudes there is more complexity, with sub-branches and re-circulations of the fronts observed (Graham et al., 2012; Kim and Orsi, 2014). In the Drake Passage and Scotia Sea these fronts partition the ocean into three major zones (Fig. 1): the Subantarctic Zone (SAZ), the Polar Front Zone (PFZ) and Antarctic Zone (AAZ) divided by the Subantarctic and Polar Fronts, as well as the Antarctic Continental Zone south of the Southern Boundary (Orsi et al., 1995; Pollard et al., 2002).

This physical zonation of the Scotia Sea and its control on the distribution of macronutrients creates a biogeochemical zonation, reflected in spatial variations in phytoplankton biomass and community structure (e.g. Holm-Hansen et al., 2004; Whitehouse et al., 2012). The poleward shoaling of density surfaces, which supports the horizontal geostrophic flow of the ACC, also brings nutrient-rich waters closer to the surface, producing positive gradients in seawater nitrate, phosphate, and silicic acid concentrations from north to south. In

addition to this, seawater silicic acid concentrations increase southwards along density surfaces, most likely due to diapycnal mixing with deeper waters that are enriched in Si by deep remineralisation of biogenic silica (Ridgwell et al., 2002).

Around the Southern Ocean as a whole, deeper (1000 to 2000 m) waters moving southwards across the ACC are balanced by an equatorward flow of 1) newly-formed dense deep and bottom waters from the Weddell Sea (Sloyan and Rintoul, 2001), and 2) lower density Antarctic Surface Water (AASW) and Winter Water (WW) in the upper layers. The AASW and WW subduct at the Polar Front and contribute to the formation of Antarctic Intermediate Water (AAIW), marked by a subsurface salinity minimum. Within the Scotia Sea, Circumpolar Deep Water (CDW) is introduced by the ACC, comprising Lower CDW (LCDW) derived from North Atlantic Deep Water (NADW) and the less dense, older Upper CDW (UCDW) sourced from the Indian and Pacific Oceans. A colder, slightly less saline variety of LCDW referred to as Southeast Pacific Deep Water (SPDW) has also been observed in the Scotia Sea, with a distinctive silicate maximum resulting from mixing with Ross Sea deep waters (Garabato et al., 2002).

In the location of the Weddell Gyre, the cold, Weddell Sea Bottom Water (WSBW) mixes upwards with warmer CDW to form Weddell Sea Deep Water (WSDW), added to by lateral advection of recently-ventilated waters from outside the Weddell Sea (Meredith et al., 2000; Ohshima et al., 2013). WSDW also forms directly from the descent and mixing of shelf waters in the Weddell Sea. WSDW is then able to exit into the Scotia Sea through deep gaps in the South Scotia Ridge, as well as flowing around the South Sandwich Islands and into the Atlantic through the Georgia Basin. This outflow represents the densest contribution to the equatorward-flowing Antarctic Bottom Waters (AABW) (Meredith et al. 2000).

## 2.2. Sampling and analytical methods

Samples were collected during the *RRS James Clark Ross* cruise JR299 in the austral autumn (March to April) 2014 and from an additional transect (JR273b) along the North Scotia Ridge (Fig. 1). Unfiltered seawater samples were collected in acid-cleaned low-density polyethylene bottles for dissolved barium, silicic acid, and nitrate and phosphate analysis using standard Niskin bottles deployed on a CTD (Conductivity-Temperature-Depth) rosette. Samples for nutrient analysis were frozen at -20°C (or at 4°C for the silicic acid samples). Samples for Ba analysis were acidified (0.1% v/v Romil UpA hydrochloric acid) and stored in cool and dark conditions.

Standard Niskin bottles are not expected to cause contamination for Ba. Additional blank samples of 18M $\Omega$ .cm Milli-Q water were processed on board under the same conditions as

samples for testing purposes: the blanks were exposed to the air of the ship for the same length of time, handled similarly around the CTD rosette and in the laboratory, acidified, and stored under the same conditions. The blanks were diluted with 3% HNO<sub>3</sub> (Romil UpA) and measured via ICP-MS, yielding signals of 0.2% and 2.5% of average spiked seawater counts (<sup>135</sup>Ba and <sup>138</sup>Ba respectively). Whilst there is a possibility that some Ba could be released into solution from suspended particles or barite crystals dissolved during storage, the maximum possible particulate contribution is still below 1% of the dissolved fraction, assuming maximum particulate Ba of 500 pmol/L in the upper water column (top ~200m) of this region of the Southern Ocean (Dehairs et al., 1997) and all particulate Ba is dissolvable.

### 2.2.1. Dissolved barium

The barium concentrations of unfiltered seawater samples were analysed by isotope dilution inductively coupled plasma mass spectrometry (ID ICP-MS) at the University of Bristol, using a Thermo-Finnigan Element-2 (Bristol Isotope Group, Earth Sciences Department). Subsamples of seawater and reference standards were spiked with a <sup>135</sup>Ba-enriched solution (10 µg/mL <sup>135</sup>Ba, Inorganic Ventures, Christiansburg, VA, USA) to a <sup>138</sup>Ba/<sup>135</sup>Ba ratio of 0.65 to 1, in order to minimize error magnification, and diluted 20-fold in 18MΩ.cm Milli-Q deionized water (to produce a final solution of approximately 3-5 nmol/kg Ba) (Pyle et al., 2017).

A mass bias correction coefficient was calculated each analysis run by measuring the ratio of <sup>138</sup>Ba/<sup>135</sup>Ba in a 1 ppb Ba natural standard solution prepared in 5% (v/v in 18MΩ.cm Milli-Q water) seawater (NASS-6), which was then compared to the average natural ratio (10.88 ± 0.02) (de Laeter et al., 2003). Blank solutions of 3% (v/v of concentrated reagent) HNO<sub>3</sub> in 18.2MΩ.cm water were analysed to correct for background Ba signal from the introduction system of the ICP-MS (<sup>135</sup>Ba blank counts <0.15% of spiked seawater sample counts; <sup>138</sup>Ba blank counts <0.5% of seawater sample counts), and a set of consistency standards were measured at regular intervals to quantify the long-term reproducibility of the measurements (Table 1). A correction for any seawater matrix effects was applied to the blank measurements by monitoring the sensitivity of a natural standard solution in 3% HNO<sub>3</sub> vs. a natural standard solution in 5% seawater, before the blanks were subtracted from sample counts.

*Table 1: Reproducibility of standards measured in Bristol from March to November 2016. Values given are twice relative standard deviation (2RSD). Determined values were corrected from moles per mass of seawater to nM assuming a seawater density of 1.025 kg/L. Errors from In-house Standard 1 (from the Scotia Sea, 100m depth) are considered applicable to the higher range of Scotia and Weddell Sea samples, whilst errors from NASS-6 can be applied to the lower range, as the average dissolved barium concentrations are the most comparable. For*

consistency, the most conservative uncertainty of 1.7 % (2RSD, from the NASS-6 standard) is applied to all samples.

<i>Standard:</i>	In-house Standard 1	NASS-5	NASS-6
2RSD	1.34%	3.26%	1.73%
<i>n</i>	72	33	70
Average [Ba] (nM)	73.5	37.4	49.3

Seawater standards of comparable barium concentration to the samples show a long-term external reproducibility of  $\pm 1.7\%$  (2RSD) or better across all analytical runs from March to November 2015 (Table 1). Within each analytical run, reproducibility of these seawater standards was  $\pm 1.1\%$  (2RSD) or better. Additional details on the analytical methods for dissolved Ba are provided in Pyle et al. (2017).

### 2.2.2. Dissolved inorganic nutrients

Dissolved inorganic nutrients (silicic acid, phosphate, and nitrate + nitrite) were analysed at the University of East Anglia using a San++ Gas Segmented Continuous Flow Analyser (Skalar, Breda, The Netherlands). The accuracy of the measured nutrient concentrations was assessed by performing a six-point calibration, using a mixed standard containing silicate, nitrate, and phosphate. Standards and wash solution were made in a saline solution containing 35 g reagent grade NaCl/L in ultrapure water. Prior to the preparation of the standards and wash solution the NaCl was baked at 400 °C to remove any nitrate contamination. The reproducibility of nitrate and nitrite (NO<sub>x</sub>), phosphate (PO<sub>4</sub>) and silicic acid (Si(OH)<sub>4</sub>) concentrations was  $\pm 1.70\ \mu\text{M}$ ,  $\pm 0.18\ \mu\text{M}$  and  $\pm 1.64\ \mu\text{M}$  (1SD) respectively, calculated by analysing eighteen sets of duplicate samples. Further details of nutrient analyses are given in the Supplementary Information.

### 2.2.3. Temperature, salinity and oxygen concentrations

Temperature, salinity, and oxygen concentrations were recorded for each CTD cast using a SBE911Plus unit with dual SBE3Plus temperature and SBE4 conductivity sensors and a Paroscientific pressure sensor, and an SBE43 oxygen sensor, and used to characterise the water masses present and identify the positions of the frontal zones (Supplementary Information).

Conductivity measurements were processed and converted to salinity, and calibrated by the regular collection of discrete seawater samples from CTD casts, analysed for salinity on board using a Guildline Autosol 8400B salinometer. Discrete samples were also collected at five

CTD stations for on board measurement of dissolved oxygen concentrations via Winkler titration, which was used to calibrate the CTD oxygen probes.

#### 2.2.4. Quantifying deviation from $Ba_d/Si(OH)_4$ trends

Where linear correlations exist between  $Ba_d$  and silicic acid, deviation above and below the line of best-fit regression is quantified by calculating  $Ba_d^{Si\ residual}$  values (Equation 1) for each profile. These systematic deviations from the observed linear relationship between  $Ba_d$  and silicic acid could result from non-conservative processes such as barite formation or dissolution that do not affect the silicon cycle. Positive  $Ba_d^{Si\ residual}$  values indicate that the  $Ba_d$  measured is higher than predicted by silicic acid values, whilst negative  $Ba_d^{Si\ residual}$  values signify that  $Ba_d$  is lower than predicted. No direct mechanistic associations are implied between the two elements, only correlation and deviation from that correlation. Note also that the uncertainty in the residual value will be location-specific, largely determined by the number of samples in each station profile.

$$Ba_d^{Si\ residual} = Ba_d^{Measured} - (m \times Si(OH)_4^{Measured} + c) \quad (1)$$

### 3. Data and results

The full range of  $Ba$  concentrations in this study varied between 42 nmol/kg and 100 nmol/kg (Fig. 2, 3). Estimates of barite saturation of surface waters (Supplementary Information) suggest near surface waters are generally undersaturated north of the Polar Front (PFZ and SAZ barite saturation index approximately 0.8, with higher values of approximately 1.0 near to islands), becoming generally more saturated towards the south (AAZ barite saturation index approximately 1.0-1.1; Weddell Sea barite saturation index approximately 1.1-1.2). There are significant positive linear correlations between  $Ba_d$  and  $NO_x$  ( $Ba_d = 2.4 \cdot NO_x + 6.6$ ;  $R^2 = 0.58$ ;  $p < 0.001$ ),  $Ba_d$  and  $PO_4$  ( $Ba_d = 28.6 \cdot PO_4 + 19.8$ ;  $R^2 = 0.44$ ;  $p < 0.001$ ) and  $Ba_d$  and silicic acid ( $Ba_d = 0.38 \cdot Si(OH)_4 + 53.9$ ;  $R^2 = 0.92$ ;  $p < 0.001$ ; Supplementary Information).

Applying a multivariate linear regression analyses of the whole dataset (Scotia and Weddell Seas and all available parameters; Fig. 2, 3) the best model fit to the data ( $p$  value  $< 0.01$ ) suggests that  $Ba_d$  concentrations could be significantly related to processes also linked to potential temperature, salinity, and silicic acid concentrations (Table 2). Separating the dataset into regions reveals more nuanced information about the role of frontal zones and water masses in the biogeochemical cycling of dissolved barium.

Table 2: Table of results from multivariate linear regression model applied to the whole  $Ba_d$  dataset. Model statistics:  $R^2 = 0.94$ ;  $p < 0.001$ . Bold values show statistically significant relationships.

	Coefficient	Standard Error	t Stat	P-value
Nitrate ( $\mu M$ )	-0.095	0.106	-0.894	0.372
Phosphate ( $\mu M$ )	0.524	1.128	0.464	0.643
Silicate ( $\mu M$ )	0.188	0.017	11.153	<0.001
Oxygen ( $\mu mol/kg$ )	-0.003	0.008	-0.327	0.744
Potential Temp	-2.530	0.238	-10.625	<0.001
Salinity	14.774	1.815	8.138	<0.001

### 3.1. Dissolved barium and macronutrients in the Scotia and Weddell Seas

#### 3.1.1. North of the Polar Front (PFZ and SAZ)

In the top 200 m  $Ba_d$  increases rapidly with depth, more closely following the behaviour of  $NO_x$  and  $PO_4$  than silicic acid, which remains fairly constant with depth (Supplementary Information; Fig. S6). The  $NO_x$  and  $PO_4$  concentrations continue to increase below 200 m at a slower rate until reaching maximum levels at approximately 1500 m, which are maintained throughout the deeper waters. In contrast, both silicic acid and  $Ba_d$  are broadly invariant between 200 and 500 m, before increasing at a similar pace until 1500 m (Fig 4a-d). The  $Ba_d$  concentrations reach maximum levels at approximately 2500 m, and silicic acid concentrations continue to rise at the deeper stations until close to bottom depths of 4000 m.

The similarity of behaviour between  $Ba_d$ ,  $NO_x$ , and  $PO_4$  in PFZ and SAZ surface waters (0 to 200 m) is replaced in intermediate waters by a more dominant similarity between  $Ba_d$  and silicic acid. Despite the marked similarity in their surface water behaviour, the overall relationships between  $Ba_d$  and  $NO_x/PO_4$  are distinctly non-linear, whilst a significant overall positive linear correlation between  $Ba_d$  and silicic acid is identified ( $Ba_d = 0.46 * Si(OH)_4 + 50.9$ ;  $n = 76$ ;  $R^2 = 0.95$ ;  $p < 0.001$ ).

These offsets from the linear relationship between  $Ba_d$  and silicic acid are shown in the  $Ba_d^{Si \text{ residual}}$  values, which are negative in surface waters and rise to values around zero over the upper 200 m. At two stations (Stations 33 and 35; Sta. 35 displayed in Fig. 4a-d) that exhibit the most depleted surface  $Ba_d$  concentrations,  $Ba_d^{Si \text{ residual}}$  values are negative at the surface and increase over the upper 200m. The  $Ba_d^{Si \text{ residual}}$  values then increase to an anomalously high maximum at 300m, decreasing thereafter to near zero at 1000m. These values then remain close

to zero through the oxygen minimum zone until they begin to increase again at ~2000m in the transition to UCDW, then decrease from 3000m to negative values again in the deepest water.

### 3.1.2. *The Antarctic Zone (AAZ)*

$Ba_d$  concentrations in the AAZ display a steady rate of increase from lower surface values (approximately 70 nmol/kg) to maximum concentrations of 95 nmol/kg at approximately 2000 m (Fig. 4e-h). Shallow sites within the ACC (top 150 m) record higher  $Ba_d$  values relative to silicic acid than the overall single-station linear regression would predict (Fig. 4f), and these samples record a shallower  $Ba_d/Si(OH)_4$  trend, indicating that  $Ba_d$  varies less with respect to silicic acid at these shallow ACC sites than it does in the intermediate depth ACC waters.

Variations in the behaviour of silicic acid and  $Ba_d$  with depth are observed in more detail in the  $Ba_d^{Si\ residual}$  values calculated from the individual  $Ba_d/Si(OH)_4$  regression at each station, which are positive in surface waters before decreasing to a negative subsurface minimum between 200 and 800 m, returning to positive values below 1000 m, and decreasing to values near zero by the bottom of the water column. The sub-surface minimum of  $Ba_d^{Si\ residual}$  values corresponds to the oxygen minimum zone, denoting both a transition into the UCDW and the depth range of maximum NOx and PO4 remineralisation (Fig. 4). A transition to a sub-surface maximum deeper in the water column but within the UCDW water mass occurs in all profiles, with the depth of that maximum increasing northwards (800 m in the south to 2200 m in the north; Fig. 4e-h).

### 3.1.3. *The North Scotia Ridge*

Stations to the west of the Polar Front, as its path curves north through Shag Rocks Passage in the North Scotia Ridge, follow a similar distribution of variables to the PFZ/SAZ and AAZ stations across the Drake Passage. Positive  $Ba_d^{Si\ residual}$  values are associated with the deeper UCDW whilst intermediate waters exhibit less scatter around the strong positive  $Ba_d/Si(OH)_4$  correlation, displaced above the global trend line. East of the Polar Front, the shallowing of UCDW and re-establishment of a strong salinity gradient are accompanied by stronger  $Ba_d^{Si\ residual}$  gradients, with positive values in surface waters and negative values from the transition to UCDW/oxygen minimum zone at 200 to 300 m, underlain by a return to positive values in the lower part of the UCDW at 1000 m (Fig. 3).

### 3.1.4. *Antarctic continental shelf waters*

Surface water  $Ba_d$  concentrations in this near-Antarctic region are relatively high compared to those in the open Southern Ocean, with the shallowest station on the continental slope reaching maximum concentrations (86 nmol/kg) in the sub-surface by 500 m, and the deeper Station 7 reaching maximum values (95 nmol/kg) at the base of the oxygen minimum zone). The  $NO_x$  and  $PO_4$  concentrations increase with depth throughout the upper 500 m and are then largely invariant throughout the rest of the water column, whilst silicic acid largely mimics the behaviour of  $Ba_d$  with depth (Fig. 5, S7). There are significant positive linear correlations between  $Ba_d$  and  $NO_x$  ( $Ba_d = 1.94 * NO_x + 26.8$ ;  $R^2 = 0.52$ ;  $p < 0.001$ ) and  $Ba_d$  and silicic acid ( $Ba_d = 0.30 * Si(OH)_4 + 60.1$ ;  $R^2 = 0.96$ ;  $p < 0.001$ ), and a weaker relationship between  $Ba_d$  and  $PO_4$  ( $R^2 = 0.17$ ;  $p = 0.007$ ) reflecting a generally weaker N-P relationship in this region. There is very little scatter in the correlation of  $Ba_d$  and silicic acid, reflected in the small variations from zero in the  $Ba_d^{Si\ residual}$  values with depth (Fig. 5a-d).

### 3.1.5. The Weddell Sea

Stations 44 and 45 lie on the edge of the Weddell Gyre, where  $Ba_d$  concentrations are consistently higher than at the Scotia Sea stations, with even the surface minima at approximately 80 nmol/kg (Fig. 5e-h). The majority of macronutrient variation is seen in the low temperature (-2 to -1 °C) waters of the upper 200 m, with both  $NO_x$  and  $PO_4$  increasing from low surface values to sub-surface maxima across a sharp salinity gradient (33.5 salinity at the surface, 35 salinity at 200 m), below which they decrease slightly throughout the bulk of the water column. Silicic acid and  $Ba_d$  concentrations do not reach sub-surface maxima until approximately 1000 m, with these values sustained over the next 2000 m until a slight decline in concentrations below depths of 3000 m. At Station 44,  $Ba_d^{Si\ residual}$  values are negative at the surface, then maintain slightly positive values from 500 to 4500 m. Station 45 exhibits more variable  $Ba_d^{Si\ residual}$  values, with zero values at the surface, negative values by 200 m that steadily rise with depth until 3500 m, remaining at consistent positive values until 4500 m. The  $Ba_d^{Si\ residual}$  values at both stations show sharp variations at the very base of the water column (4500 to 4750 m; Fig. 5e-h).

## 4. Discussion

Although the  $Ba_d$  distributions from our study are in general agreement with the global distributions of macronutrients, when examined in detail these relationships are revealed to be more complex. The deviations from the linear correlation between  $Ba_d$  and silicic acid in surface waters (Fig. 4-5), and the co-variation of  $Ba_d$  and  $NO_x/PO_4$  north of the Polar Front (Fig. S6),

implies that the surface cycling of barium depends on factors that also influence dominant phytoplankton ecology. In intermediate and deeper waters, the departures from the linear relationship of  $Ba_d$  and silicic acid offer insight into the barium and barite cycling, and the transitions between characteristic water masses (Fig. 4-5).

#### *4.1. Linking the distributions of $Ba_d$ and macronutrients: a global view*

##### *4.1.1. Non-linear global relationship between $Ba_d$ and $NO_x$ or $PO_4$*

Throughout the global ocean there is a non-linear positive correlation between  $Ba_d$  and the macronutrients  $NO_x$  and  $PO_4$ , with three broad observations: (1)  $NO_x$  and  $PO_4$  show consistent drawdown in surface waters, whilst the behaviour of  $Ba_d$  in surface waters varies between regions; (2)  $NO_x$  and  $PO_4$  quickly reach subsurface maxima which they usually sustain through intermediate depth waters, whilst the  $Ba_d$  maximum is both deeper and more variable in depth; (3)  $NO_x$  and  $PO_4$  concentrations decrease with depth through deeper waters whilst  $Ba_d$  remains constant or continues to increase. With the exception of HNLC regions,  $NO_x$  and  $PO_4$  are limiting nutrients for primary productivity, with concentrations depleted to nanomolar levels in subtropical surface waters (Moore et al., 2013). Even in HNLC regions such as large parts of the Southern Ocean, both  $NO_x$  and  $PO_4$  still experience surface drawdown, but without reaching fully depleted levels, with phytoplankton growth instead limited by silicic acid, micronutrients, or the availability of light. In contrast,  $Ba_d$  never reaches surface concentrations lower than 30 nmol/kg, and in some ocean basins (the North Atlantic and the North Pacific) it shows an invariant profile in the top few hundred metres where macronutrients show strong drawdown (Hsieh and Henderson, 2017).

A certain degree of surface drawdown of  $Ba_d$  is consistent with uptake of barium by phytoplankton into an intracellular pool, consistent with observations of labile Ba associated with spring phytoplankton blooms (Ganeshram et al., 2003; Paytan and Griffith, 2007) and the observation of high cellular Ba concentrations (Fisher et al., 1991). However, the lack of a consistent stoichiometric relationship to macronutrients suggests either a highly variable uptake into organic matter, depending for example on plankton community structure, or differing degrees and rates of remineralisation between  $Ba_d$  and macronutrients. These differences are again evident in the depth profiles of  $Ba_d$  compared to  $NO_x$  and  $PO_4$ , which show relatively shallow remineralisation as particulate organic matter is broken down by microbes or zooplankton in the oxygen minimum zone and  $NO_x$  and  $PO_4$  are remineralised. In contrast,  $Ba_d$  concentrations, although increasing with depth, generally do so at a slower rate over a much

larger depth range, implying regeneration in parallel with the slower dissolution of phytoplankton biominerals.

#### 4.1.2. *The positive linear correlation between $Ba_d$ and silicic acid, and variations between ocean basins*

The positive linear relationship observed between  $Ba_d$  and silicic acid throughout the global ocean (Fig. 6) is highly significant and overall exhibits modest overall scatter ( $Ba = 0.58 * Si(OH)_4 + 39.33$ ;  $n = 322$ ;  $R^2 = 0.94$ ;  $p < 0.01$ ). However, understanding how and where deviations in this  $Ba_d/Si(OH)_4$  relationship occur, and variations in the  $Ba_d/Si(OH)_4$  relationship between different ocean basins, can provide insight into the level of interaction between silicon and barium cycling. Although some regions display regressions that deviate little from the overall relationship (the South Atlantic, South Pacific, and Indian Oceans), others have a distinctive regional signal (the Equatorial Pacific, the North Atlantic and the North Pacific). The Southern Ocean has been shown by numerous studies (Jeandel et al. 1996; Jacquet et al. 2007; Hoppema et al. 2010; data presented here for the Scotia Sea) to exhibit lower slopes and higher intercepts than are observed in other regions (Fig. 6; Table 3).

Investigations in the Southern Ocean have suggested that, although barite does form in non-diatom-dominated regions, its precipitation is favoured where these siliceous organisms make up a significant fraction of the material exported from the surface layer (Bishop, 1988). This observation may be explained if enhanced TEP or polysaccharide availability, from the remains of diatom frustules, provide a more suitable microenvironment for barite precipitation than the remains of other phytoplankton (Martinez-Ruiz et al., 2018); if the enhanced ballasting effect of diatom frustules increases settling rates and reduces Ba recycling in surface waters; or, indeed, because diatom abundance and barite precipitation are coincidentally linked via a third mechanism e.g. physical water column conditions that favour diatom growth also favour barite precipitation. However, the role of non-siliceous organic matter in the removal of  $Ba_d$  from the surface has been observed in the field (Pyle et al., 2017) and confirmed by laboratory production of barite from axenic coccolithophorid cultures, without the presence of opal or fecal pellet packaging (Ganeshram et al., 2003). A combination of the possible explanations presented above may explain why the presence of diatoms tends to be associated with enhanced  $Ba_d$  drawdown (e.g. Esser and Volpe, 2002): barium and sulphate may be associated equally with all phytoplankton or their decayed products, but will sink more rapidly when associated with diatom frustules due to the ballasting of larger or more heavily silicified cells (Tréguer et al., 2018). As this organic matter is exported to the reported depths of barite formation (200 to

2000 m) (Bates et al., 2017; Dehairs et al., 2008; Horner et al., 2015; Van Beek et al., 2007), it may tend to form aggregates containing microenvironments that are more susceptible to barite precipitation than organic matter originating from other phytoplankton groups. At greater depths, or at the sediment surface, both barite and opal dissolve, allowing vertical mixing to define the Ba-silicic acid relationships.

*Table 3: Summary of studies investigating  $Ba_d$  vs.  $Si(OH)_4$  in the global ocean compared to the Southern Ocean. WAP = West Antarctic Peninsula.*

Location	Slope coefficient	$R^2$	P	Reference
North Indian Ocean	0.56	-	-	Jeandel et al. 1996
South Indian Ocean	0.25	-	-	Jeandel et al. 1996
Indian Ocean	0.63	0.98	<0.001	GEOSECS (MELVILLE) 1978
North Pacific	0.66	0.93	<0.001	GEOSECS (MELVILLE) 1973
Equatorial Pacific	0.74	0.99	<0.001	GEOSECS (MELVILLE) 1973/4
South Pacific	0.56	0.96	<0.001	GEOSECS (MELVILLE) 1974
North Atlantic	0.75	0.95	<0.001	GEOSECS (KNORR) 1972
South Atlantic	0.55	0.86	<0.001	GEOSECS (KNORR) 1972/3
145°E PFZ-AZ	0.23±0.01	0.72	<0.001	Jacquet et al. 2007
145°E SAF-PFZ	0.31±0.01	0.91	<0.001	Jacquet et al. 2007
Prime Meridian	0.2645	0.909	-	Hoppema et al. 2010
Weddell Sea	0.2322	0.806	-	Hoppema et al. 2010
WAP all	0.21	0.716	<0.001	Pyle et al., 2016
WAP surface	0.14	0.266	<0.001	Pyle et al., 2016
JR299 all	0.40	0.92	<0.001	This study; JR299 (2014)
Drake Passage S.PF	0.32	0.90	<0.001	This study; JR299 (2014)
Drake Passage N.PF	0.46	0.96	<0.001	This study; JR299 (2014)
Weddell Sea	0.15	0.60	<0.001	This study; JR299 (2014)

## 4.2. Linking the distributions of $Ba_d$ and macronutrients in the Scotia Sea

### 4.2.1. $Ba_d$ and silicic acid in the Scotia Sea

Within different water masses, there are significant changes in  $Ba_d^{Si\text{ residual}}$  with depth, indicating that non-conservative processes are important in most of the study region, in addition to water mass mixing (Supplementary Information; Fig. S9; Fig. 4, 5). However, it is challenging to determine the relative impact of the different non-conservative processes, barite

precipitation and silica dissolution, on  $Ba_d^{Si\text{ residual}}$  values. Recent measurements of barium isotopes in the tropical North Atlantic and South Atlantic (Bates et al., 2017; Horner et al., 2015) have established the utility of combining  $Ba_d$  and silicic acid concentrations with barium isotope measurements ( $\delta^{137/134}Ba$ ), as the preferential incorporation of light isotopes during barite formation makes the isotopic signature of the remaining water mass sensitive to barite cycling, but unaffected by silicate cycling (Cao et al., 2016; Hsieh and Henderson, 2017; Von Allmen et al., 2010). In the absence of ( $\delta^{137/134}Ba$ ) measurements, useful insights can still be made about barium cycling in this region by investigating deviation from linearity in  $Ba_d$  - silicic acid relationships, and the comparison of these trends to global patterns (Fig. 6).

There is a clear shift in the behaviour of  $Ba_d$  in the upper 100m of the water column as the Drake Passage and North Scotia Ridge transects cross the Polar Front. This is observed not only in the near-surface profiles of  $Ba_d$ , but in the changing sign of surface  $Ba_d^{Si\text{ residual}}$  values (negative to positive, travelling from north to south across the PF), indicating a change in the observed relationship between  $Ba_d$  and silicic acid across this frontal divide (Fig. 4).

North of the Polar Front in the PFZ/SAZ there is noticeable drawdown of  $Ba_d$  in surface waters despite these waters being likely undersaturated with respect to barite in the majority of the region, most pronounced at Stations 33 and 35 where fluorescence indicates a high level of productivity (Fig. S10). These lowered surface concentrations then follow the pattern of  $NO_x$  and  $PO_4$  concentrations, increasing rapidly over the upper 100m of the water column. This suggests an association at these stations between  $Ba_d$  and the rapidly remineralised particulate organic carbon tracked by  $NO_x$  and  $PO_4$ . In contrast, in the waters south of the Polar Front in the AAZ, the enrichment of  $Ba_d$  from surface minimum concentrations down through the water column is at a much slower rate than for any of the macronutrients (e.g. in the AAZ in the top 1000m, only approximately 30% of the overall Ba remineralisation is complete compared to 100% of the  $PO_4$ ), and shows no distinct behaviour in the top 100m (Supplementary Information; Fig S8).

Surveys of the Southern Ocean have established the presence of a clear biogeochemical divide between the northerly waters of the PFZ and SAZ, and the AAZ waters south of the polar front (Marinov et al., 2008). There is a distinct change in phytoplankton assemblage across the Polar Front, with nanoflagellates to the north and diatoms dominating to the south (Hinz et al., 2012; Mengelt et al., 2001), consistent with cross-front differences in the observed distributions of  $Ba_d$ . In the nanoflagellate-dominated waters north of the divide there appears to be an association between  $Ba_d$  and the organic matter of the organisms that is not observed elsewhere in the Scotia Sea, or indeed in any other stations throughout the global ocean. It is difficult to assess what the nature of this organic matter association might be, as a mechanism for the

active uptake of barium into cells is not known (Paytan and Griffith, 2007). However, cellular Ca transporters rarely distinguish strongly against co-transport of Ba (Krejci et al., 2011), and we postulate that barium uptake occurs in these surface waters in association with cells or organic matter that is not diatom-generated, and is then remineralised at shallow depths. This behaviour parallels NO<sub>x</sub> and PO<sub>4</sub> only in the upper 100m, below which the Ba<sub>d</sub> distribution resumes a more silica-like profile, indicating that the generally observed correlation between Ba<sub>d</sub> and skeletal material still occurs in this region, in layers below this unusual surface activity (Supplementary Information; Fig. S6).

During the spring and summer months, diatom blooms are prevalent in the silicic acid and iron limited AAZ waters, consuming silicic acid and causing the silicate front to migrate southwards (Franck, 2000; Hiscock et al., 2003; Landry et al., 2002). As these samples were collected during austral autumn, the background productivity of these diatom-dominated waters was relatively low, with substantial surface silicic acid concentrations extending northwards to just south of the polar front. Nevertheless, there is some silicic acid drawdown at the surface, and while there is also Ba<sub>d</sub> drawdown, the removal is less than predicted by the overall Ba-silicate regression for each station (Fig. 4). The persistence of a slight positive Ba<sub>d</sub><sup>Si residual</sup> signal in the very surface layer of the AAZ waters highlights this deviation from the observed Ba-silicic acid relationship over the depth range of maximum primary production.

#### 4.2.2. Barium in intermediate waters (200-2000m): the overprinting of large scale circulation by barite cycling

Although intermediate waters tend to agree with the global linear correlation between Ba<sub>d</sub> and Si(OH)<sub>4</sub>, there are notable deviations with depth at individual stations. There is a seasonally-variable transition in phytoplankton communities between the diatom-dominated colder AAZ waters and the nanoflagellate-dominated warmer waters of the PFZ and the SAZ (Hinz et al., 2012; Mengelt et al., 2001). However, the Ba<sub>d</sub> signals in intermediate waters (between 100 to 200m and 2000m) reflect not only the recycling of any biologically related phases of barium sinking from the surface, but also any vertical mixing between laterally transported water masses. It is also likely that the majority of biologically-mediated barite precipitation occurs within this depth range. The changing Ba<sub>d</sub><sup>Si residual</sup> values recorded across known water mass transitions is a key tool for de-convolving these different signals.

The multivariate linear regression analysis of the whole dataset suggests that the Ba<sub>d</sub> distribution was most significantly linked to the distributions of salinity, temperature, and silicic acid. The predictive power of these parameters can be attributed to the distinct variation in Ba<sub>d</sub>

distributions between water masses – not only the horizontal gradient of  $Ba_d$  across the frontal zones of the Scotia Sea, but the variation with depth as the cores of vertically layered water masses are sampled.

North of the Polar Front in the PFZ/SAZ,  $Ba_d$  shows a strong linear relationship with salinity, indicating an important role of water mass mixing (Supplementary Information; Fig. S5). Surface waters in the PFZ subduct to form AAIW, with initially invariant silicic acid and  $Ba_d$  concentrations that mix at its base with the higher concentrations of UCDW. South of the Polar Front, the oxygen-poor UCDW lies directly below the surface waters, deepening from south to north, and recording a steady increase in silicic acid and  $Ba_d$  concentrations with depth. The  $Ba_d$  and silicic acid gradients within this water mass, and the shift towards positive  $Ba_d^{Si\ residual}$  values (Supplementary Information; Fig. S9), indicates the occurrence of in-situ dissolution of barite co-occurring with diatom frustules, potentially with a depth-gradient in input from deep Pacific waters that carry a notable excess of  $Ba_d$  relative to silicic acid.

There appear to be two different types of  $Ba_d/Si(OH)_4$  deviations occurring within the UCDW. This is most distinct south of the Polar Front, where there is a large negative  $Ba_d^{Si\ residual}$  signal recorded between 100 and 1000m (Fig. 4f), denoting a relative depletion in  $Ba_d$  as surface waters transition to UCDW. As the surface waters here also have a relative  $Ba_d$  excess due to silicic acid uptake by diatoms, this cannot be a result of the mixing of UCDW and surface waters, but must instead reflect a separate process. The co-location of this  $Ba_d$  depletion horizon with the oxygen minimum zone, and the subsurface maxima of  $NO_x$  and  $PO_4$  is highly suggestive that this  $Ba_d$  depletion relative to silicic acid results from microbially-mediated barite precipitation (Dehairs et al., 1997; Gonzalez-Muñoz et al., 2012; González-Munoz et al., 2003; Jacquet et al., 2007). This precipitation would transfer barium from the dissolved to the particulate pool, and although the concentrations concerned are likely to be too small to show up as a localised minimum in  $Ba_d^{Si\ residual}$  (Jacquet et al., 2007), the fact that this process does not involve any change in the silicic acid pool could potentially cause the negative swing in  $Ba_d^{Si\ residual}$  values within the upper few hundred meters (Fig. 4-5).

Whilst this feature is clear in the AAZ waters, north of the Polar Front the pattern of  $Ba_d^{Si\ residual}$  values is more complex. The negative residual signatures in surface waters (particularly at the highly productive Stations 33 and 35) are underlain here by the broadly uniform AAIW, within which  $Ba_d$  and silicic acid appear to become correlated again once the surface drawdown of  $Ba_d$  has been returned to the dissolved pool by dissolution of sinking barite. At Stations 33 and 35, there is suggestive evidence of the profiles tending towards negative residual values at the oxygen minimum zone, where the rate of organic matter remineralization and potential Ba-

binding to phytoplankton TEP, polysaccharides, or bacterial EPS is at a maximum rate. Generally, however, the intermediate waters are dominated by the positive UCDW signal.

This could be an indication of reduced barite formation at mesopelagic depths in waters north of the Polar Front relative to south, which could be directly linked to the shift in overlying phytoplankton assemblages and to the magnitude of export production and rate of sinking in the two regions. The surface water drawdown of  $Ba_d$  north of the Polar Front does not seem to translate to a higher formation of barite at depth, with much of the  $Ba_d$  instead being recycled initially at shallower depths in the water column. This shallower remineralisation could also be aided by the lower barite saturation state within the surface waters of the SAZ and PFZ. It appears that the specific association of  $Ba_d$  with siliceous organisms, coupled with the ballasting power of the large or heavily silicified diatom frustules (Tréguer et al., 2018), enables the transport of Ba to depths greater than in areas dominated by other sinking phytoplankton.

#### 4.2.3. Deep waters of the Scotia Sea

In deeper waters (2000 to 4000 m)  $Ba_d$  concentrations reach an asymptotic value and then show little variation down to the base of the water column in all of the regions investigated. Deeper stations in the Drake Passage record a slight decrease in  $Ba_d$  values at the base of the water column, with a simultaneous increase in silicic acid concentrations and resulting negative excursion in  $Ba_d^{Si\text{ residual}}$  values that marks the presence of Southeast Pacific Deep Water (SPDW; Fig. 2). The distinctive silicate maximum associated with this colder, slightly fresher sub-set of LCDW is thought to originate from mixing with Ross Sea deep waters (Garabato et al., 2002), and it appears that these waters may also inherit relatively low  $Ba_d$  concentrations, possibly due to a low Ba content in sinking organic particles (DeMaster et al., 1992; McManus et al., 2002). Both north and south of the Polar Front, the preservation of a consistent Ba maximum indicates that at these depths the exchange between the particulate and dissolved barium pools is at steady state, in contrast to silicic acid concentrations, which generally continue to increase until the base of the water column. This observation could be explained by i) different relative saturation states of barite within organic matter micro-environments or in seawater (as barite saturation state increases with depth) and silica in deepwater (undersaturated globally in the oceans), or ii) because the more soluble barite particles have already dissolved from sinking aggregates at shallower depths in the water column, leaving only the more massive or less soluble particles, while biogenic silica continues to dissolve even within the upper sediments. The latter interpretation is supported by the observation that biogenic barite preserved in sediments is less

soluble in acid digestions than barite in water column samples (Bridgestock et al., 2018; Dymond et al., 1992; Eagle et al., 2003).

#### 4.3. *The Weddell Sea: a region of barite supersaturation?*

In most regions of the global oceans, near-surface seawater is undersaturated with respect to barite, as saturation state is a function of barium and sulphate concentrations, temperature, salinity and pressure (Monnin et al., 1999; Rushdi et al., 2000). Our estimates of barite saturation index for the surface waters of the Weddell Sea may be a notable exception, where open ocean surface waters may become supersaturated with respect to pure barite (saturation index approximately 1.1-1.2, likely reaching a maximum at Station 44; Supplementary Information; Fig. S10), in agreement with previous findings (Jeandel et al., 1996; Monnin et al., 1999). Barite precipitation from solution, without the need for biologically-derived micro-environments, may explain the excursions in  $Ba_d^{Si\text{ residual}}$  values in the upper 200 m of the southern-most Weddell Sea Station 44 (Fig. 5e-h).

#### 5. Summary and conclusions

There is a positive linear correlation between  $Ba_d$  and silicic acid throughout the global ocean water column, a link which is not seen between  $Ba_d$  and the other macronutrients. An exception to this general rule is observed in the surface waters of the Scotia Sea north of Polar Front, where the distribution of  $Ba_d$  appears more similar to that of  $NO_x$  and  $PO_4$  than silicic acid in the upper 100 m, suggesting an unusual association between  $Ba_d$  and primary production in surface waters in this region. This could be explained by near-surface Ba uptake by adsorption, cellular incorporation or potentially barite formation, which is rapidly dissolved as it sinks out of the surface layer.

The globally-observed linear relationship between silicic acid and  $Ba_d$  may result solely from co-location in the formation and recycling of separate and distinct carrier phases, coupled with the effects of large-scale ocean circulation. In support of this, the data presented here suggest that the  $Ba_d$  distribution in the Scotia Sea is largely controlled by transitions between distinct water masses, each with slightly differing relationships between  $Ba_d$  and silicic acid. However, the signature of barite formation at mesopelagic depths, and dissolution in the deeper water column, can also be distinguished in  $Ba_d/Si(OH)_4$  deviations that overprint these larger scale circulation patterns. Variation in the degree of implied biogenic barite formation across the Polar Front suggests a correlation between phytoplankton assemblage and barium cycling, as enhanced barium drawdown in subsurface waters is observed south of the Polar Front, where

the phytoplankton community shifts to one dominated by diatoms. This could be a significant consideration in the application of the  $Ba_{\text{excess}}$  proxy for past export production (Paytan and Griffith, 2007), as increases in sedimentary barite concentrations may be related to changes in phytoplankton community structure as well as absolute increases in the export of organic matter produced in surface waters.

These insights into the effects of surface phytoplankton community structure on the formation of barite in the subsurface could be investigated further through barium isotope analysis. Such isotopic measurements could verify whether or not deviations in the observed  $Ba_d/Si(OH)_4$  relationship observed in intermediate waters are the result of changes in barite precipitation, re-dissolution and water mass mixing (e.g. Bates et al., 2017). If rates of biogenic barite precipitation are controlled more by community structure than by net primary productivity, as indicated here, then this could have important consequences for the use of sedimentary barite as a proxy for export production.

#### Acknowledgements

We would like to thank the captain and crew of the RRS James Clark Ross. KMP was supported by a NERC PhD Studentship. Many thanks to Christopher D. Coath for help in the laboratory. The labwork and barium analyses were funded by a grant to KH (EU FP7\_PEOPLE-20120CIG Proposal number 320070). KH is also funded by a Royal Society University Research Fellowship.

Figure 1: Sites of depth profiles collected during cruise JR299 in the Scotia Sea and Weddell Sea (Bathymetry etopo1). Approximate positions of fronts marked by dashed lines: Subantarctic Front (SAF), Polar Front (PF), Southern ACC Front (SACCF) and Southern Boundary (SB). Stations north of the Polar Front (Subantarctic Zone SAZ and Polar Front Zone PFZ; JR299 Stations 30-40 from the Drake Passage Section and Stations 101-132 from the North Scotia Ridge Section) are marked with yellow squares. Stations south of the Polar Front are marked with red diamonds (Antarctic Zone AAZ; Stations 95-100 from the North Scotia Ridge Section). Stations south of the Southern Boundary are marked by green triangles (continental shelf waters adjacent to the Peninsula; stations 2-7) and white circles (Weddell Sea; Stations 44-45). White numbers show station numbers of examples plotted in profile in Figures 4 and 5.

Figure 2: Drake Passage section. Colour scale represents labelled parameters in each panel; locations of Southern Boundary (SB) and Polar Front (PF) marked by vertical dotted purple lines. Stations and sampling events are marked with black dots; station numbers are labelled along the

top of the top panel. Delineation of water masses schematically marked for reference: Weddell Sea Deep Water (WSDW), South Pacific Deep Water (SPDW), Lower and Upper Circumpolar Deep Water (LCDW and UCDW), Antarctic Intermediate Water (AAIW), and Antarctic Surface Water (AASW). a.  $Ba_d$  concentrations (nmol/kg); b.  $Ba_d^{Si\ residual}$  values (nmol/kg); c. dissolved oxygen concentrations ( $\mu\text{mol/kg}$ ); d. salinity; e. potential temperature ( $^{\circ}\text{C}$ ).

Figure 3: North Scotia Ridge section. Colour scale represents labelled parameters in each panel; a.  $Ba_d$  concentrations (nmol/kg); b.  $Ba_d^{Si\ residual}$  values (nmol/kg); c. dissolved oxygen concentrations ( $\mu\text{mol/kg}$ ); d. salinity; e. potential temperature ( $^{\circ}\text{C}$ ). Stations and sampling events are marked with black dots; station numbers are labelled along the top of the top panel.

Figure 4: a-d. Example depth profiles of Drake Passage waters north of the Polar Front in the SAZ/PFZ (Station 30 black circles; Station 35 red triangles; Station 40 green squares) a. Dissolved oxygen concentrations ( $\mu\text{mol/kg}$ ); b.  $Ba_d^{Si\ residual}$  values (nmol/kg); c. Dissolved barium concentrations (nmol/kg); d. Silicic acid ( $\mu\text{M}$ ). Shaded area represents the oxygen minimum zone. e-h. Example depth profiles of ACC waters south of the Polar Front in the AAZ (Station 11 black circles; Station 13 red triangles; Station 26 green squares) e. Dissolved oxygen concentrations ( $\mu\text{mol/kg}$ ); f.  $Ba_d^{Si\ residual}$  values (nmol/kg); g. Dissolved barium concentrations (nmol/kg); h. Silicic acid ( $\mu\text{M}$ ). Shaded area represents the oxygen minimum zone (note OMZ marginally deeper at Station 26).

Figure 5: a-d. Example depth profiles of Antarctic continental shelf waters south of the Southern Boundary (Station 3 black circles; Station 5 red triangles; Station 7 green squares) a. Dissolved oxygen concentrations ( $\mu\text{mol/kg}$ ); b.  $Ba_d^{Si\ residual}$  values (nmol/kg), zero line marked by black dotted line for reference; c. Dissolved barium concentrations (nmol/kg); d. Silicic acid ( $\mu\text{M}$ ). e-h. Depth profiles of Weddell Sea stations (Station 44 black circles; Station 45 red triangles) e. Dissolved oxygen concentrations ( $\mu\text{mol/kg}$ ); f.  $Ba_d^{Si\ residual}$  values (nmol/kg); g. Dissolved barium concentrations (nmol/kg); h. Silicic acid ( $\mu\text{M}$ ). Shaded area represents the oxygen minimum zone.

Figure 6: Scatter plots of dissolved barium (nmol/kg) vs. silicic acid ( $\mu\text{mol/kg}$ ) for biogeographical divisions of the dataset, superimposed upon the global GEOSECS dataset (Ostlund, 1987), plotted in grey circles. Note our new data are in good agreement with the GEOSECS dataset. Data from the Drake Passage Transect a. Stations south of the Southern Boundary (yellow circles), ACC stations south of the PF (green circles); b. Stations north of the PF (blue circles). c. Data from the Weddell Sea (red circles). d. Data from the North Scotia Ridge Transect (cyan circles).

Supplementary data

Supplementary material

References

- Bates, S.L. et al., 2017. Barium isotopes reveal role of ocean circulation on barium cycling in the Atlantic. *Geochimica et Cosmochimica Acta*, 204: 286-299.
- Bishop, J.K.B., 1988. The barite-opal-organic carbon association in oceanic particulate matter. *Nature*, 332: 341-343.
- Bridgestock, L. et al., 2018. Controls on the barium isotope compositions of marine sediments. *Earth and Planetary Science Letters*, 481: 101-110.
- Cao, Z., Siebert, C., Hathorne, E.C., Dai, M. and Frank, M., 2016. Constraining the oceanic barium cycle with stable barium isotopes. *Earth and Planetary Science Letters*, 434: 1-9.
- Cardinal, D. et al., 2005. Variations of carbon remineralisation in the Southern Ocean illustrated by the Ba xs proxy. *Deep Sea Research Part I: Oceanographic Research Papers*, 52(2): 355-370.
- Collier, R. and Edmond, J., 1984. The trace element geochemistry of marine biogenic particulate matter. *Progress in Oceanography*, 13: 113-199.
- Cunningham, S., Alderson, S., King, B. and Brandon, M., 2003. Transport and variability of the Antarctic circumpolar current in drake passage. *Journal of Geophysical Research: Oceans*, 108(C5).
- de Laeter, J.R. et al., 2003. Atomic weights of the elements. Review 2000 (IUPAC Technical Report). *Pure and applied chemistry*, 75(6): 683-800.
- Dehairs, F., Chesselet, R. and Jedwab, J., 1980. Discrete suspended particles of barite and the barium cycle in the open ocean. *Earth and Planetary Science Letters*, 49: 528-550.
- Dehairs, F. et al., 2008. Barium in twilight zone suspended matter as a potential proxy for particulate organic carbon remineralization: Results for the North Pacific. *Deep Sea Research Part II: Topical Studies in Oceanography*, 55(14): 1673-1683.
- Dehairs, F., Shopova, D., Ober, S., Veth, C. and Goeyens, L., 1997. Particulate barium stocks and oxygen consumption in the Southern Ocean mesopelagic water column during spring and early summer: relationship with export production. *Deep Sea Research Part II: Topical Studies in Oceanography*, 44(1-2): 497-516.
- DeMaster, D.J. et al., 1992. Cycling and accumulation of biogenic silica and organic matter in high-latitude environments: the Ross Sea. *Oceanography*, 5(3): 146-153.
- Dymond, J., Suess, E. and Lyle, M., 1992. Barium in deep-sea sediment: A geochemical indicator of paleoproductivity. *Paleoceanography*, 7: 163-181.
- Eagle, M., Paytan, A., Arrigo, K.R., van Dijken, G.L. and Murray, R.W., 2003. A comparison between excess barium and barite as indicators of carbon export. *Paleoceanography*, 18: Art. no. 1021.
- Esser, B.K. and Volpe, A.M., 2002. At-sea high-resolution chemical mapping: extreme barium depletion in North Pacific surface water. *Marine chemistry*, 79(2): 67-79.
- Fisher, N.S., Guillard, R.R. and Bankston, D.C., 1991. The accumulation of barium by marine phytoplankton grown in culture. *Journal of marine research*, 49(2): 339-354.
- Franck, V.M., 2000. Iron and silicic acid concentrations regulate Si uptake north and south of the Polar Frontal Zone in the Pacific Sector of the Southern Ocean. *Deep-Sea Research II*, 47: 3315-3338.
- Ganeshram, R.S., Francois, R., Commeau, J. and Brown-Leger, S.L., 2003. An experimental investigation of barite formation in seawater. *Geochimica et Cosmochimica Acta*, 67: 2599-2605.

- Garabato, A.C.N., McDonagh, E.L., Stevens, D.P., Heywood, K.J. and Sanders, R.J., 2002. On the export of Antarctic bottom water from the Weddell Sea. *Deep Sea Research Part II: Topical Studies in Oceanography*, 49(21): 4715-4742.
- Gonzalez-Muñoz, M., Martinez-Ruiz, F., Morcillo, F., Martin-Ramos, J. and Paytan, A., 2012. Precipitation of barite by marine bacteria: A possible mechanism for marine barite formation. *Geology*, 40(8): 675-678.
- González-Munoz, M.T. et al., 2003. Precipitation of barite by *Myxococcus xanthus*: possible implications for the biogeochemical cycle of barium. *Applied and Environmental Microbiology*, 69(9): 5722-5725.
- Graham, R.M., Boer, A.M., Heywood, K.J., Chapman, M.R. and Stevens, D.P., 2012. Southern Ocean fronts: Controlled by wind or topography? *Journal of Geophysical Research: Oceans*, 117(C8).
- Hinz, D. et al., 2012. Comparative seasonal biogeography of mineralising nannoplankton in the Scotia Sea: *Emiliana huxleyi*, *Fragilariopsis* spp. and *Tetraparma pelagica*. *Deep Sea Research Part II: Topical Studies in Oceanography*, 59: 57-66.
- Hiscock, M.R. et al., 2003. Primary productivity and its regulation in the Pacific Sector of the Southern Ocean. *Deep-Sea Research II*, 50: 533-558.
- Holm-Hansen, O. et al., 2004. Temporal and spatial distribution of chlorophyll-a in surface waters of the Scotia Sea as determined by both shipboard measurements and satellite data. *Deep-Sea Research II*, 51: 1323-1331.
- Hoppema, M. et al., 2010. Distribution of barium in the Weddell Gyre: Impact of circulation and biogeochemical processes. *Marine Chemistry*, 122(1): 118-129.
- Horner, T.J., Kinsley, C.W. and Nielsen, S.G., 2015. Barium-isotopic fractionation in seawater mediated by barite cycling and oceanic circulation. *Earth and Planetary Science Letters*, 430: 511-522.
- Hsieh, Y.-T. and Henderson, G.M., 2017. Barium stable isotopes in the global ocean: Tracer of Ba inputs and utilization. *Earth and Planetary Science Letters*, 473: 269-278.
- Jacquet, S., Dehairs, F., Cardinal, D., Navez, J. and Delille, B., 2005. Barium distribution across the Southern Ocean frontal system in the Crozet–Kerguelen Basin. *Marine Chemistry*, 95(3): 149-162.
- Jacquet, S., Dehairs, F., Elskens, M., Savoye, N. and Cardinal, D., 2007. Barium cycling along WOCE SR3 line in the Southern Ocean. *Marine Chemistry*, 106(1): 33-45.
- Jacquet, S. et al., 2008. Mesopelagic organic carbon remineralization in the Kerguelen Plateau region tracked by biogenic particulate Ba. *Deep Sea Research Part II: Topical Studies in Oceanography*, 55(5): 868-879.
- Jeandel, C., Dupre, B., Lebaron, G., Monnin, C. and Minster, J.-F., 1996. Longitudinal distributions of dissolved barium, silica and alkalinity in the western and southern Indian Ocean. *Deep Sea Research Part I: Oceanographic Research Papers*, 43(1): 1-31.
- Jullion, L., Jacquet, S. and Tanhua, T., 2017. Untangling biogeochemical processes from the impact of ocean circulation: First insight on the Mediterranean dissolved barium dynamics. *Global Biogeochemical Cycles*.
- Kim, Y.S. and Orsi, A.H., 2014. On the variability of Antarctic Circumpolar Current fronts inferred from 1992–2011 altimetry. *Journal of Physical Oceanography*, 44(12): 3054-3071.
- Krejci, M.R. et al., 2011. Selectivity in biomineralization of barium and strontium. *Journal of structural biology*, 176(2): 192-202.
- Landry, M.R. et al., 2002. Seasonal dynamics of phytoplankton in the Antarctic Polar Front region at 170° W. *Deep Sea Research Part II: Topical Studies in Oceanography*, 49(9): 1843-1865.
- Lea, D.W., 1993. Constraints on the alkalinity and circulation of glacial circumpolar deep-water from benthic foraminiferal barium. *Global Biogeochemical Cycles*, 7: 695-710.

- Lea, D.W. and Boyle, E.A., 1989. Barium content of benthic foraminifera controlled by bottom-water composition. *Nature*, 338: 751-753.
- Marinov, I. et al., 2008. Impact of oceanic circulation on biological carbon storage in the ocean and atmospheric pCO<sub>2</sub>. *Global Biogeochemical Cycles*, 22: GB3007, doi:10.1029/2007GB002958.
- Martinez-Ruiz, F. et al., 2018. Barium bioaccumulation by bacterial biofilms and implications for Ba cycling and use of Ba proxies. *Nat Commun*, 9.
- McManus, J., Dymond, J., Dunbar, R.B. and Collier, R.W., 2002. Particulate barium fluxes in the Ross Sea. *Marine geology*, 184(1): 1-15.
- Mengelt, C. et al., 2001. Phytoplankton pigment distribution in relation to silicic acid, iron and the physical structure across the Antarctic Polar Front, 170° W, during austral summer. *Deep Sea Research Part II: Topical Studies in Oceanography*, 48(19): 4081-4100.
- Meredith, M.P. et al., 2000. On the sources of Weddell Gyre Antarctic bottom water. *Journal of Geophysical Research: Oceans*, 105(C1): 1093-1104.
- Monnin, C., Jeandel, C., Cattaldo, T. and Dehairs, F., 1999. The marine barite saturation state of the world's oceans. *Marine Chemistry*, 65(3): 253-261.
- Moore, C. et al., 2013. Processes and patterns of oceanic nutrient limitation. *Nature Geoscience*, 6(9): 701.
- Nurnberg, C.C., Bohrmann, G., Schluter, M. and Frank, M., 1997. Barium accumulation in the Atlantic sector of the Southern Ocean: results from 19,000 year records. *Paleoceanography*, 12: 594-603.
- Ohshima, K.I. et al., 2013. Antarctic Bottom Water production by intense sea-ice formation in the Cape Darnley polynya. *Nature Geoscience*, 6(3): 235-240.
- Orsi, A.H., Whitworth, T. and Nowlin, W.D., 1995. On the meridional extent and fronts of the Antarctic Circumpolar Current. *Deep Sea Research Part I: Oceanographic Research Papers*, 42(5): 641-673.
- Ostlund, H.G., 1987. *GEOSECS Atlantic, Pacific, and Indian Ocean Expeditions Vol 7*.
- Paytan, A. and Griffith, E.M., 2007. Marine barite: Recorder of variations in ocean export productivity. *Deep Sea Research Part II: Topical Studies in Oceanography*, 54(5-7): 687-705.
- Pollard, R.T., Lucas, M.I. and Read, J.F., 2002. Physical controls on biogeochemical zonation in the Southern Ocean. *Deep-Sea Research II*, 49: 3289-3305.
- Pyle, K. et al., 2017. Coastal barium cycling at the West Antarctic Peninsula. *Deep Sea Research Part II: Topical Studies in Oceanography*, 139: 120-131.
- Ridgwell, A.J., Watson, A.J. and Archer, D.E., 2002. Modeling the response of the oceanic Si inventory to perturbation, and consequences for atmospheric CO<sub>2</sub>. *Global Biogeochemical Cycles*, 16: Art. no. 1071.
- Rushdi, A.I., McManus, J. and Collier, R.W., 2000. Marine barite and celestite saturation in seawater. *Marine Chemistry*, 69(1): 19-31.
- Sloyan, B.M. and Rintoul, S.R., 2001. The Southern Ocean limb of the global deep overturning circulation. *Journal of Physical Oceanography*, 31(1): 143-173.
- Sternberg, E., Tang, D., Ho, T.-Y., Jeandel, C. and Morel, F.M., 2005. Barium uptake and adsorption in diatoms. *Geochimica et Cosmochimica Acta*, 69(11): 2745-2752.
- Thomas, H. et al., 2011. Barium and carbon fluxes in the Canadian Arctic Archipelago. *Journal of Geophysical Research: Oceans*, 116(C9).
- Tréguer, P. et al., 2018. Influence of diatom diversity on the ocean biological carbon pump. *Nature Geoscience*, 11(1): 27.
- Van Beek, P. et al., 2007. 228 Ra/226 Ra and 226 Ra/Ba ratios to track barite formation and transport in the water column. *Geochimica et cosmochimica acta*, 71(1): 71-86.

- Von Allmen, K., Böttcher, M.E., Samankassou, E. and Nägler, T.F., 2010. Barium isotope fractionation in the global barium cycle: First evidence from barium minerals and precipitation experiments. *Chemical Geology*, 277(1): 70-77.
- Whitehouse, M. et al., 2012. Substantial primary production in the land-remote region of the central and northern Scotia Sea. *Deep Sea Research Part II: Topical Studies in Oceanography*, 59: 47-56.

#### Highlights

- Barium cycling in the Scotia Sea is influenced by both water mass mixing and non-conservative processes
- Barium and macronutrients relationships shift as a result of shifts in phytoplankton assemblages
- Multiple controlling factors have implications for the use of barium as a productivity proxy

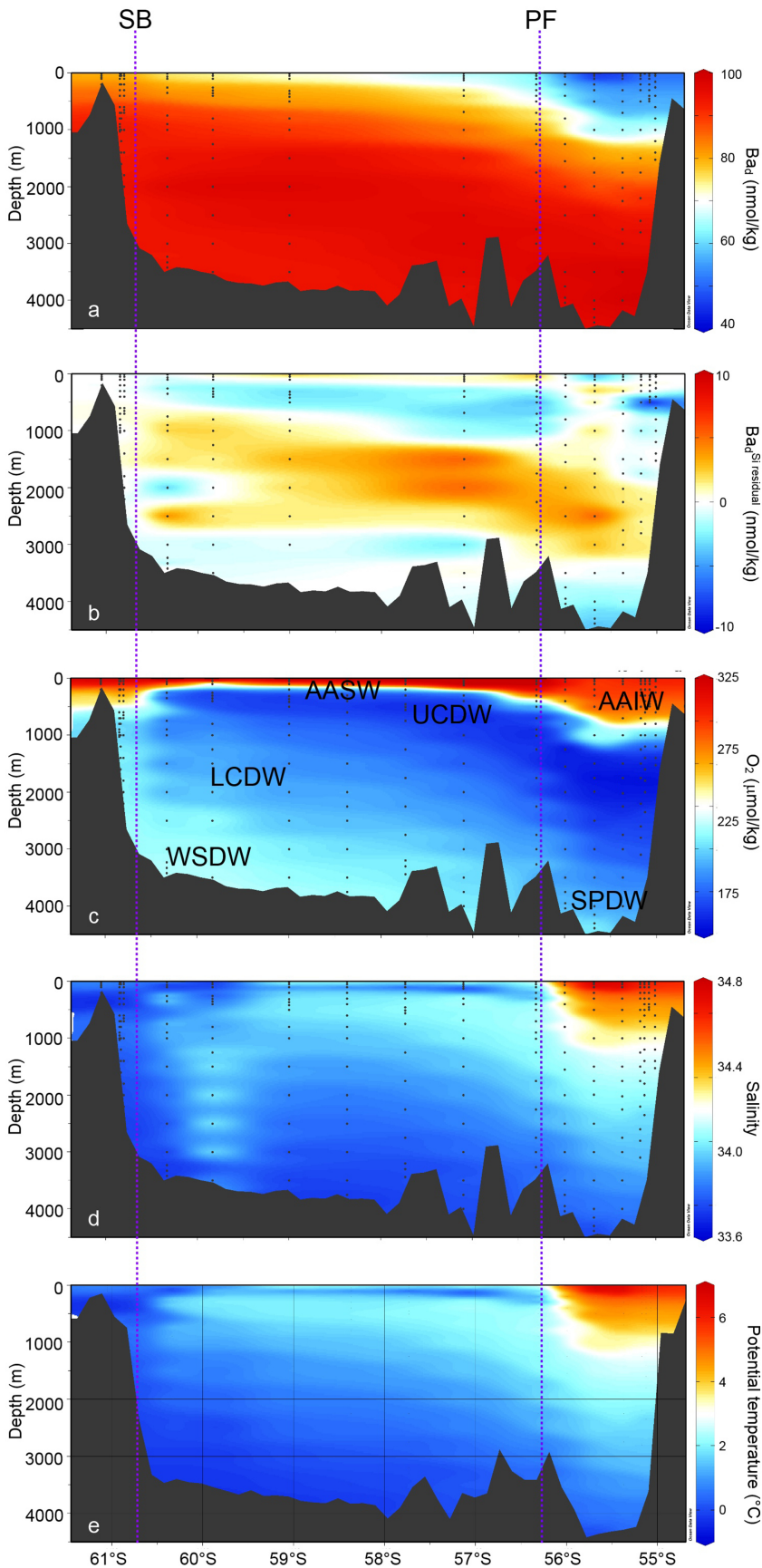


Figure 1

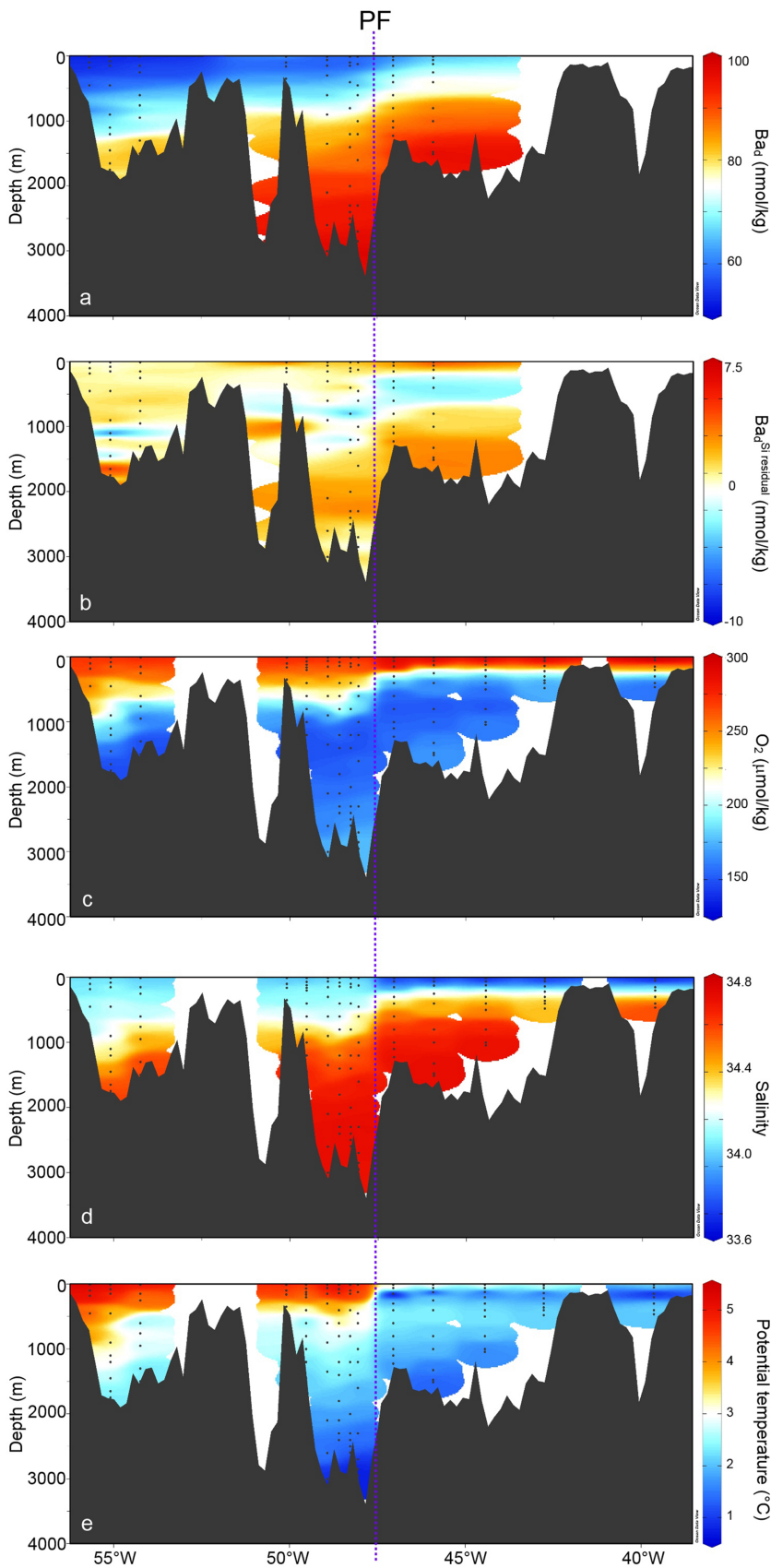


Figure 2

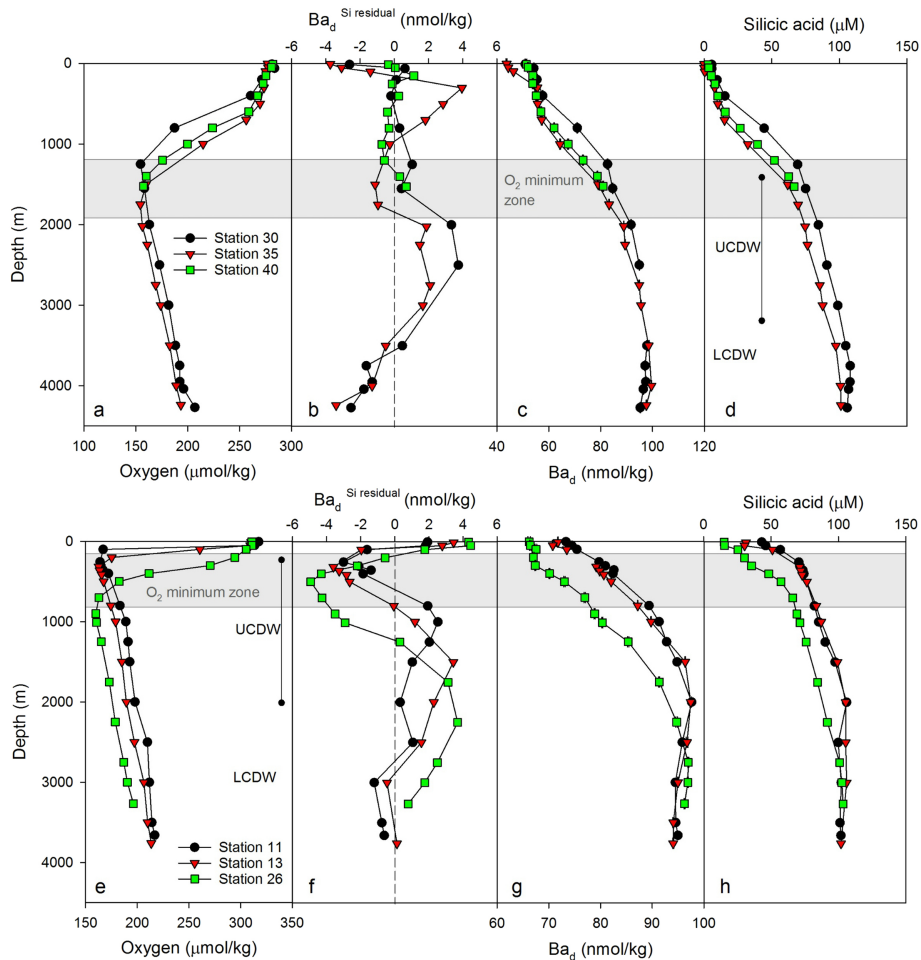


Figure 3

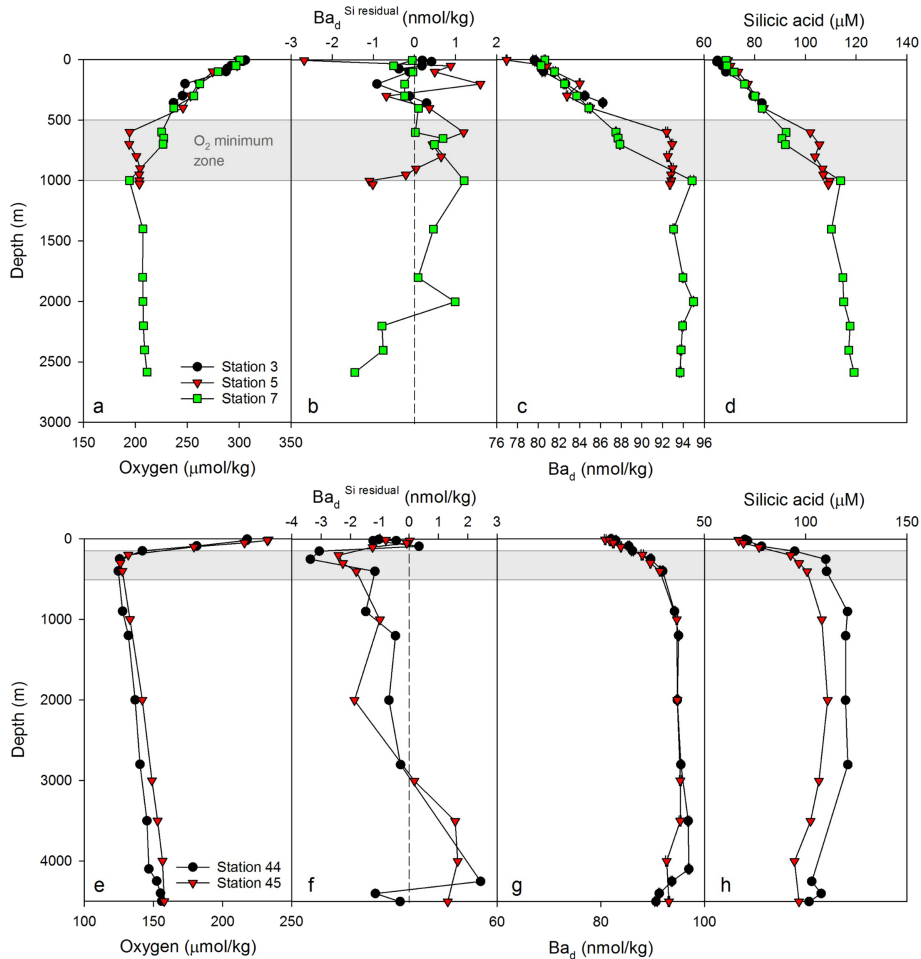


Figure 4

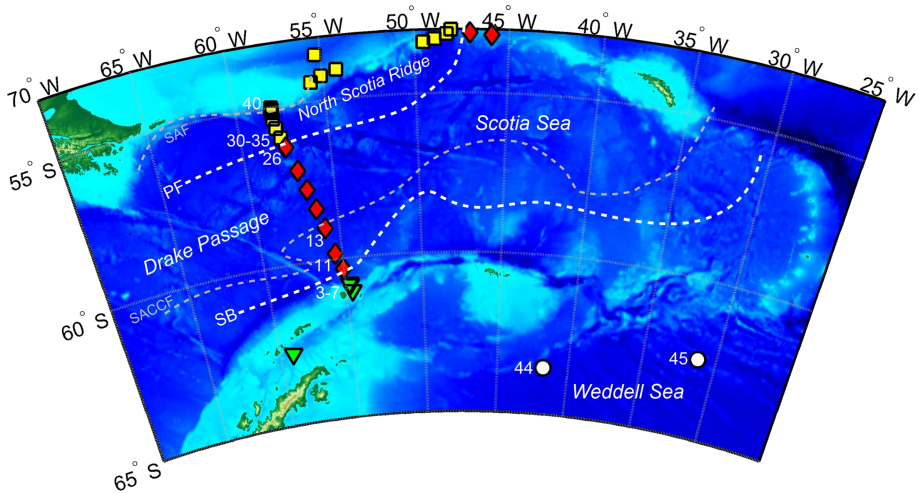


Figure 5

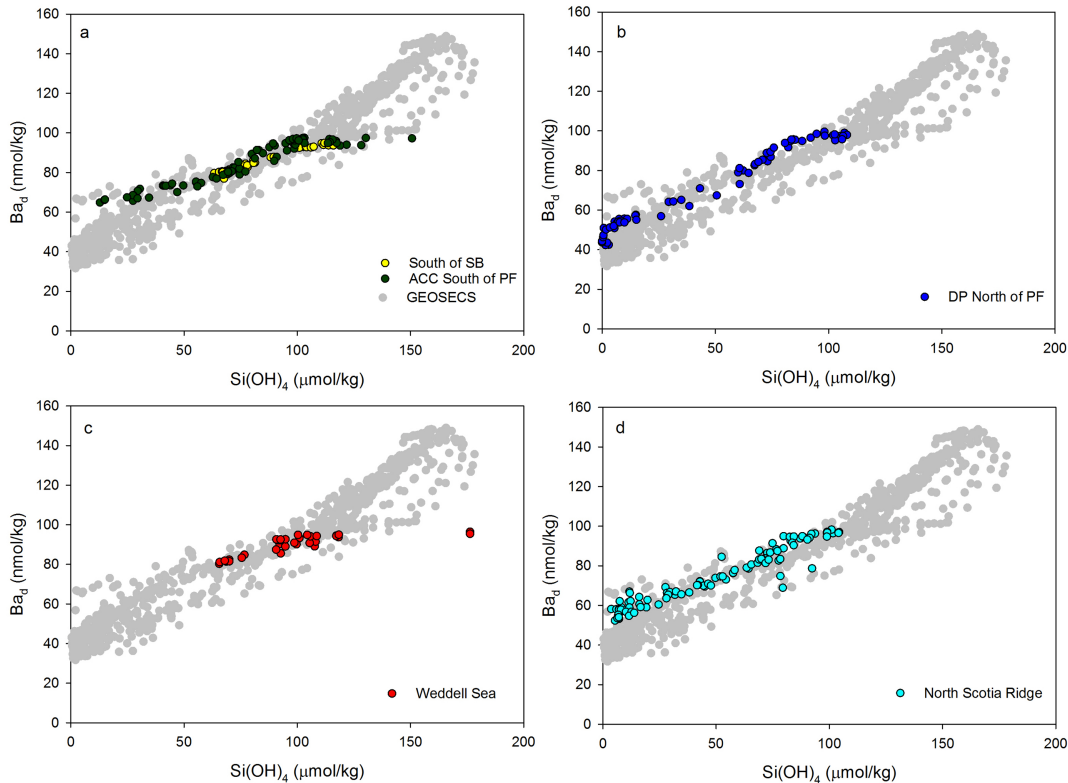


Figure 6